Role of Interfaces and Contact Formation for the Application of Lead-Free Perovskite Materials in Photovoltaic Cells

Jonas Horn and Derck Schlettwein*

Perovskite solar cells (PSCs) represent a promising approach toward a climate-neutral energy supply. Great progress has been made to reach attractive efficiencies of photovoltaic cells at rather low energy input. However, the toxicity of today´s most efficient materials combined with their chemical instability even when assembled to devices poses unsolved problems. Alternative materials have been developed but up to now cannot compete in efficiency. In many instances, such lack of efficiency is caused by problems in contact formation. Aside from reports in cell architecture, a number of studies have focused on the specific investigation of contact phenomena, also in lateral geometry. Chemical reactivity at interfaces and migration of ions in contacts and within the perovskite materials lead to significant hysteresis in electron conduction and photovoltaic properties. Herein, recent results on such investigations for lead-free perovskite materials are reviewed. The main findings of contact formation with these materials are summarized and the specific impact of different methods of analysis is discussed. By these means, the hope is to provide a good starting ground for groups with new approaches to materials chemistry or device architecture as well as to groups with new approaches to device analysis.

1. Introduction

To address the increasing global demand for electrical energy, the search for sustainable and renewable energy technologies is one of the biggest challenges to minimize the global impact on the climate. Because the incident solar irradiation on our planet surpasses the global need for energy by far,[1] using this available energy appears to be one of the most feasible solutions. This fact, in combination with a strong reduction of cost for photovoltaic power generation of around 80% during the last decade,

has led to a large global investment in solar energy of 1.3 trillion dollars,[2] yielding its prominent position in covering future electrical energy demand.[3] The estimated global technical potential, taking into account already established solar energy technologies, exceeds the global demand for primary energy by a factor of 3–100.[1] To compete with nonrenewable sources of energy, further cost reduction and improvement of energy conversion are of great relevance. Third-generation photovoltaics are widely regarded as a potential candidate to achieve such further improvements.[4] The power efficiency of lab-scale perovskite solar cells (PSCs), as one member of third-generation photovoltaics, showed a remarkable increase from 3.8%[5] to over 25%[6] within around 10 years, making them the most promising candidates amongst these not-yet-established photovoltaic technologies to revolutionize the market. The mixed organic–metal–halide perovskite with the formula ABX_3, where A stands for an organic (or inorganic) cation, B represents a metal cation, usually Pb(II) or Sn(II), and X a halide anion (Cl^-, I^-, Br^-), acts as an absorber layer in such PSCs and is, therefore, responsible for many of the advantageous properties of these devices. Along with the high cell efficiencies reached, the rather low energy input in cell preparation[7] leads to attractively low energy payback times[8,9] and expected harvesting factors,[7] fundamental prerequisites for a sustainable large-volume energy technology. Further, the rather low active mass of the semiconductor layers needed in the cells and acceptable availability of the elements in the earth's crust needed to construct the cells[10] lead to great promise held in PSCs as a sustainable energy technology.

However, apart from the long term stability of lead-based PSCs, which is far from reaching a competitive level,[11] and the need to upscale preparation processes[12] (e.g., by the use of roll-to-roll-processes[13]), the containment of eco-toxic lead is regarded as a major obstacle on the way of PSCs toward our rooftops or solar parks.[14–17] One way to circumvent the latter is to replace Pb(II) by other group(IV) metals such as Sn(II), yielding a rather similar material with widely comparable optoelectronic properties[18,19] (e.g., charge carrier lifetimes, excitonic binding energies, absorption coefficients, bandgap energy), however at the cost of further reduction of ambient stability due to facile

J. Horn, D. Schlettwein
Institute of Applied Physics and Center of Materials Research
Justus Liebig University Giessen
Heinrich-Buff-Ring 16, 35392 Giessen, Germany
E-mail: schlettwein@uni-giessen.de

The ORCID identification number(s) for the author(s) of this article can be found under https://doi.org/10.1002/pssr.202100369.

oxidation of Sn^{2+} to Sn^{4+}, acting as a strong p-type dopant with consequently increased carrier density[20] and nonradiative recombination rates, which negatively affects the solar cell performance.[21–24] Sn(II) performs especially well when combined with the organic cation formamidinium ($CH(NH_2)_2^+$, FA) and iodide and, like the Pb(II) analogue, shows tunable properties by exchanging the halide or the organic part.[18,19,25] Optimization in composition of the absorber layer, preparation methods, and interfacial engineering enabled researchers to push the PCE above 14%,[26–28] which is the highest value for a lead-free PSC, however far from competing with the records reached for lead-based devices. Another intensely researched group of materials from this perspective is the so-called double perovskites $A_2B'B''X_6$, where the divalent Pb(II) ion (B) is replaced by one monovalent (B') and one trivalent (B'') ion, e.g., Ag(I) and Bi(III), in structures of alternating metal centers. When combined with Cs^+ (A) and Br^- (X), the fully inorganic perovskite $Cs_2AgBiBr_6$ is obtained.[29,30] Unlike Pb(II) or Sn(II) perovskites, $Cs_2AgBiBr_6$ is remarkably stable even under ambient conditions; however, it has only limited potential as an absorber layer due to its indirect bandgap and, therefore, low absorption coefficient within the solar spectrum.[31,32]

Heterointerfaces of any given perovskite absorber to adjacent semiconducting or metallic contact materials are of great relevance,[33,34] as it generally is the case in thin-film devices, e.g., organic solar cells or organic light emitting diodes. Heterointerfaces by definition represent an interruption of the crystal lattice, as opposed to n- and p-doped regions of a given material in classical homojunctions, and therefore, represent a dominating recombination site in such thin film devices.[34] These interfaces are needed, however, for selective carrier extraction, to minimize interfacial recombination losses, and to establish a built-in electric field, necessary at least in the charge-selective layers[25] to facilitate separation and transport of photogenerated carriers toward the external circuit.[34] It is further known that ions (mostly halide anions[35]) can move rather freely within perovskite lattices due to their chemically "softness," yielding accumulation of mobile species at the aforementioned interfaces following illumination or external bias application.[36,37] The vast majority of such reports and excellent review articles are focused on contacts to lead perovskites. As an extension, this review is focused on the discussion of interfaces to lead-free perovskites, their influence on device performance, and their deliberate manipulation to improve layer and device properties. Some joint properties but also some differences to lead-based perovskites are elaborated/discussed/focused upon.

2. Experimental Methods to Study Characteristics of Contacts and Interfaces

The dependence of the observed current density on the applied voltage (j–V characteristics) serves as one of the most relevant tools to analyze the quality of a given photovoltaic cell by revealing characteristic parameters such as the open-circuit photovoltage V_{OC}, the short-circuit photocurrent density j_{SC}, the position of the maximum power point, and the fill factor FF. Further, these measurements provide first direct access to contact

characteristics in analyzing, e.g., the series resistance R_{SC} and shunt resistance R_{sh} and indicating the extent of recombination. Already in the early stages of the development of PSCs it was reported that the general shape of the j–V characteristics of PSCs is influenced by the scan rate, scan direction, and pretreatment of the cell[38] or the perovskite layer.[36,37] Despite numerous studies, a consensus about the explanation of such hysteresis is not yet reached. Various approaches are evaluated, involving migration of mobile ions within the perovskite films, ferroelectric behavior (formation of domains with alternating polarization, which is strongly debated in the literature[39–43]) of the perovskite, or trapping and detrapping of charge carriers within the perovskite. The current knowledge on hysteresis phenomena is summarized in extended reviews;[44–47] however, these are mostly focused on lead-based perovskites. A comprehensive discussion of hysteresis in lead-free PSCs, e.g., based on tin or silver and bismuth, is still missing. Therefore, we summarize the current literature status regarding hysteresis in devices of these promising lead-free materials and, further, focus on their interfaces because these are prominent contributors to the observed hysteresis phenomena. Apart from the observation of j–V characteristics in solar cell geometries or in lateral devices,[37,48] impedance spectroscopy serves as an important tool to investigate effects taking place on various timescales,[36,49] as it is the case for electric polarization and the migration of ions, both of which are suspected to influence hysteresis characteristics. The standard (and most simple) equivalent circuit used to describe impedance spectra in PSCs consists of a resistor (R_S, related to cell series resistance), in series with an RC element consisting of the geometric capacitance (C_g) and the high-frequency resistance (R_{HF}, related to recombination), and a low-frequency RC element.[50] The latter is usually related to the processes at the interface, e.g., to moving ions modifying the interfacial capacitance because their mobility is low compared to the electronic mobility in PSCs. For the description of more complex spectra, e.g., involving a negative capacitance, equivalent circuits including an inductive element, which is related to surface charging following external bias application due to moving ions, are necessary for a correct interpretation of the results.[51] Interfacial charging can be monitored independently by optical spectroscopy if, e.g., subtle changes in transmission can be monitored under a changing bias voltage across an interface, speaking in favor of partial reduction or oxidation of the materials in the interface.[52] To gain a mechanistic understanding of these phenomena, surface-sensitive methods to obtain band energies, work function, and the surface potential are of great relevance. Results of photoelectron spectroscopy (PES) and Kelvin probe force microscopy (KPFM) as discussed in this review are contributing substantially in this respect. The former was intensively applied to lead-based perovskites, resulting in very valuable information about the chemical composition and variation,[53,54] valence and conduction band energies, as well as the work function of the perovskite,[55] which can then be related to energy levels of possible contact materials[56] to study the energy-level alignment.[57] KPFM measures the surface potential and, by additional referencing, the work function with nanometer resolution[58] and, therefore, yields an alternative access to the energy-level alignment and the interface of perovskites, even at high local resolution, both laterally and

vertically. KPFM was extensively used, e.g., to map compositional variations within perovskite grains[59] and to measure the potential drop inside a PSC[60,61] and the formation of interfacial charges and mobility of ions within the perovskite layer,[62,63] as also reviewed recently.[64] Most of these measurements concentrated on lead-based materials, whereas results on lead-free perovskites and their interfaces are discussed in the following.

3. Results and Discussion of Hysteresis and Contact Characteristics

3.1. Studies on Tin-Based Perovskites

3.1.1. Origins of Hysteresis

Similar to lead-based perovskites, hysteresis effects have been observed in tin-based systems, which could be expected due to the very similar crystal structures coming along with similar defect formation energies as well as similar trap states,[65] which can be populated and depopulated. Iwamoto and co-workers described current–voltage hysteresis for illuminated methylammonium tin iodide ($MASnI_3$) layers sandwiched between indium tin oxide (ITO) and aluminum. During the scan in the positive direction, they observed an increase in current for the scan back to 0 V. In contrast, when sweeping the bias in the negative direction, a decreased current was found for the bias sweep back to 0 V (**Figure 1**a). The observations are explained by trap states (tin vacancies), which are populated for the scan in the positive direction (smaller current, Figure 1c), which in turn leads to an increased current during the scanning back to 0 V, as these trap states are already populated (Figure 1d). When the bias is swept in the negative direction below 0 V, the filled traps are depopulated (Figure 1d) and subsequently filled for the scan back to 0 V, yielding a decreased current compared to the scan from 0 to −4 V (Figure 1c).[66] We note that these observations were made for devices with a rather small electrode distance of 160 nm, resulting in strong electric fields upon application of 4 V bias and breakdown of the device for higher voltages. The capacitance,

obtained by impedance spectroscopy, showed a sharp increase at around 3 V when the traps were getting populated. This increased capacitance stayed widely constant during reverse scanning; additional injected carriers contributed to the observed current rather than being trapped to increase the capacity. Application of a sufficiently negative bias yields detrapping of carriers and subsequent reduction of the capacity (Figure 1b). Similar studies in the same group were conducted on PSCs of $MASnI_3$ contacted by C_{60} and poly(3,4-ethylenedioxythiophene)-poly(styrenesulfonate) (PEDOT:PSS) and investigated via impedance, I–V scans, and optical transmission spectroscopy.[52] Varying capacity and hysteresis upon bias sweeping in the cell were confirmed and explained by reversible electron trapping in the interface with C_{60}.

For $FASnI_3$ films deposited on symmetric interdigitated gold electrodes (electrode distance 40 μm), we observed symmetric j–V hysteresis upon bias sweeping with increased current density upon each reversal of scan direction (**Figure 2**a), which is comparable to the findings of Iwamoto in the positive scan direction, only.[67] Prolonged application of positive bias resulted in increased j during poling (Figure 2b) and persistently increased j following scan reversal toward decreasing positive potentials (Figure 2c). Strongly decreased current density (and hysteresis) was found for subsequent negative bias but preserved hysteresis behavior for repeated positive bias (Figure 2c). In summary, strongly rectifying characteristics were observed following such poling for the originally symmetric device. Due to the symmetric characteristics without poling (Figure 2a) and the asymmetric characteristics subsequent to such poling (Figure 2c), we attributed our findings to modification of charge injection at the gold–perovskite interfaces due to migration of mobile ions yielding a decreased charge transfer resistance at the interface in the direction of poling. Two different timescales were observed for the increase in current density: a fast component observed within a given scan (<1 s) and a slow component (>20 s) indicated by an increase of j during polarization (Figure 2b). We attributed these observations to slow (most likely tin vacancies) and faster moving ions (iodide vacancies) within the perovskite film.[67]
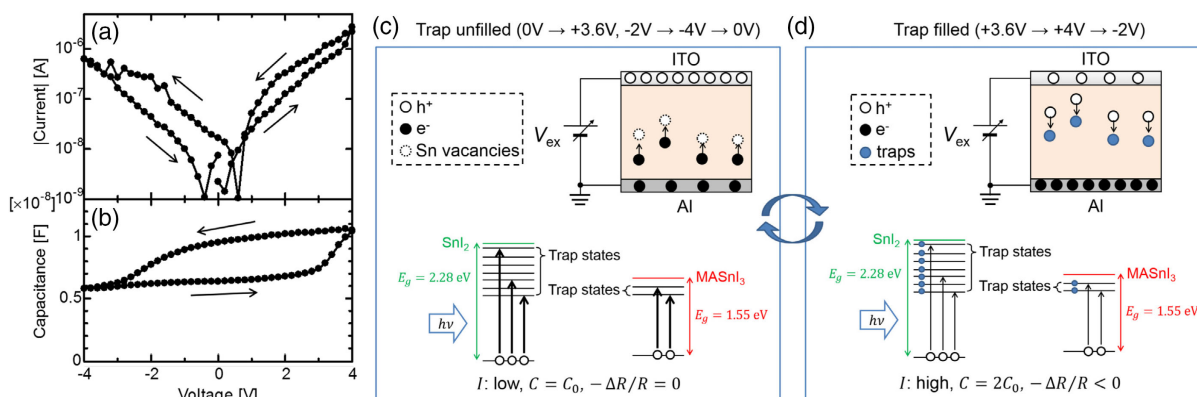

Figure 1. a) I–V scans of $MASnI_3$ between ITO and Al, showing pronounced hysteresis, depending on the scan direction. b) C–V characteristics obtained by impedance spectroscopy. c,d) Schematics of trapping and detrapping under illumination and during bias application. a–d) Reproduced with permission.[66] Copyright 2018, AIP Publishing.
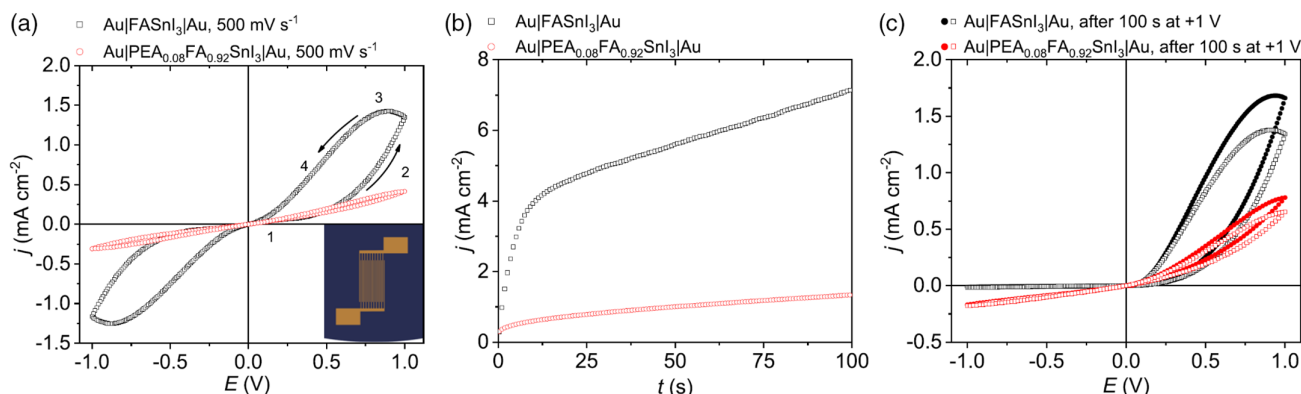
Figure 2. a) Comparison of j–V characteristics of $FASnI_3$ and $PEA_{0.08}FA_{0.92}SnI_3$ layers, which are obtained by a symmetrical lateral electrode structure and contacted with gold electrodes. b) Current density during application of a positive bias of 1 V. c) j–V characteristics after such prolonged polarization. a–c) Reproduced under the terms of the CC-BY Creative Commons Attribution 4.0 International license (https://creativecommons.org/licenses/by/4.0)[67] 2019, The Authors, published by American Institute of Physics.

3.1.2. Decrease of Hysteresis by 2D Perovskite Interlayers and/or Improved Crystallinity

The structure of lead- as well as tin-based perovskite thin films can be modified by partial substitution of the organic cation (MA^+, FA^+) by larger cations to induce the (partial) growth of 2D Ruddlson Popper perovskite phases, forming mixed 2D/3D perovskite structures.[68,69] Apart from yielding improved stability,[70] this mixing can improve the homogeneity of the (3D) perovskite and stabilize the interface to the underlying substrate.[68] We used this approach to specifically modify the interface of the perovskite with the electrode substrate by mixing $FASnI_3$ with the larger organic cation phenylethylammonium (PEA), leading to a drastically reduced j, which indicates a lower bulk defect density resulting from improved film growth, as shown previously for tin-[71] and lead-based perovskites.[70,72] Further, the hysteresis was widely suppressed, accompanied by an almost linear j–V relation (Ohmic behavior), indicating effective passivation of the interface between the electrode and perovskite by the 2D interlayer (red lines in Figure 2a). As shown by the red lines in Figure 2b, a smaller increase of j was found upon poling and the persistent hysteresis (Figure 2c) was much smaller as well following partial replacement of FA by PEA in $FASnI_3$.

Suppression of hysteresis upon interfacial modification was also reported when mixing phenylethylammonium bromide with formamidinium iodide in the preparation of tin-based absorber layers in solar cell geometry.[73] The almost identical j–V characteristics for forward and reverse scan and, technically perhaps even more important, significant improvement of the PCE (**Figure 3**a), as opposed to pronounced hysteresis observed for purely 3D Sn-based perovskite absorbers (Figure 1a, Figure 3a) were explained by the improved crystallization yielding a decreased density of trap states at the interface. The density of trap states was calculated from V_{TFL} measured in hole-only devices (Figure 3b), which confirmed the beneficial effect on the interface of PEA introduction. Similarly, the complete absence of hysteresis in tin-based cells was reported by Loi and co-workers by replacing 8% of formamidinium iodide (FAI) by phenethylammonium iodide (PEAI).[71] Such interfacial modifications using large organic cations are currently one of the most promising ways to improve the stability as well as PCE of tin-based PSCs, and an overview focusing on the detailed effects can be found elsewhere.[69]

A different form of hysteresis was observed in $FASnI_3$-based PSCs by Yu et al., resulting in a decrease of V_{oc} under reverse bias sweeping when compared to forward sweeping
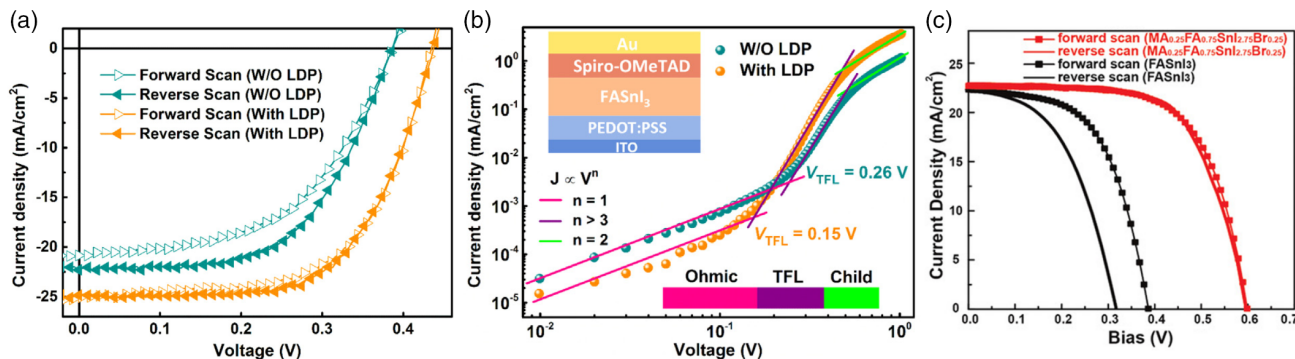

Figure 3. a) j–V scans of PSCs with and without a low-dimensional perovskite (LDP) interlayer. Whereas cells without the interlayer show pronounced hysteresis, PSCs with LDP are widely free from hysteresis and show improved PCE. b) j–V scans of a hole-only device, showing reduced trap density for LDP layers indicated by reduced V_{TLF}. c) j–V scans of PSCs using $FASnI_3$ and $MA_{0.25}FA_{0.75}SnI_{2.75}Br_{0.25}$, with the former showing sincere hysteresis. a,b) Reproduced with permission.[73] Copyright 2018, Elsevier Inc. c) Reproduced with permission.[74] Copyright 2020, Wiley-VCH.

(Figure 3c),[74] in contrast to the reduced fill factor observed earlier (Figure 3a).[73] This hysteresis could be widely suppressed by changing the stoichiometry of the perovskite material by partial substitution of FAI by MABr in the perovskite precursor solution. This yields a mixed $MA_{0.25}FA_{0.75}SnI_{2.75}Br_{0.25}$ perovskite absorber with a slightly increased bandgap but a substantially increased V_{oc}, whereas the j_{sc} remains almost constant.[74] Similar to previous interpretations, the reduced hysteresis (and improved PCE) was mainly attributed to improved film crystallinity, coming along with decreased defect and trap densities, as shown by the j–V characteristics of hole-only-devices. Decreased defect and trap densities both can reduce hysteresis: the former as it prohibits ion migration because defects are needed for this process and the latter as populating and depopulating of trap states within the bulk or at the interface can lead to j–V hysteresis (Figure 1).

3.1.3. Analysis of Contact Formation

Another perspective on the interface of a given perovskite with a contact material of interest can be obtained by observing changes of the work function upon deposition of the electron- or hole-transporting layer. Such measurements have been performed for $FASnI_3$ in contact with the electron conductor C_{60} because this is the commonly used electron-transport material (ETM) in tin-based PSCs, by either KPFM[75] or PES.[76]

Aside from an analysis of the work function of a given material, KPFM as a probe of high local resolution allows us to link results of spatial inhomogeneities of the work function with the topography of films and interfaces. This way we were able to resolve the inhomogeneous growth of C_{60} for small deposition rates on $FASnI_3$, yielding large agglomerates of C_{60} grains and poor surface coverage. This resulted in contributions of different species to the sample work function (**Figure 4**a), namely, of a monolayer of C_{60} covering the perovskite (dashed fit line centered at 4.25 eV, assignment confirmed by the green line obtained for 1 nm of C_{60} on $FASnI_3$) and agglomerates at the grain boundaries of the perovskite (dashed red line centered at 4.37 eV).[75] In contrast, good coverage was achieved for sufficiently large deposition rates, yielding only one Gaussian contribution in the work function histogram (blue line in Figure 4a,

sequence of film thicknesses in Figure 4b). By the stepwise deposition and intermittent KPFM measurements, establishment of an extended space charge layer (>90 nm) and upward bending of the conduction band (lowest unoccupied molecular orbital (LUMO) level) in C_{60} were observed by a steadily increasing work function upon further deposition (Figure 4c). The band bending deviated from the expected Mott–Schottky characteristics and was interpreted as resulting from a modification by interfacial reactions, most likely of iodide ions migrating into the electron-transport layer.

By the use of PES, Boehm et al. directly showed such migration of I^- into C_{60} upon deposition on $FASnI_3$, as the corresponding X-ray photoelectron spectroscopy (XPS) signals were observed for a thickness up to 25 nm (**Figure 5**), whereas other characteristic perovskite signals (e.g., Sn) vanished upon continued deposition of C_{60}. They further showed that I^- (618.75 eV) is converted to I_2 and I_3^- (619.75 eV), yielding n doping of C_{60} at the interface to $FASnI_3$ (Figure 5c) in good agreement with the KPFM results discussed earlier (Figure 4c). Apart from doping the C_{60} layer, such migration of I^- further led to an estimated I^- deficiency of 75% within the top first 5 nm of the $FASnI_3$ film assuming a nonuniform distribution.[76] Correspondingly, the valence band of $FASnI_3$ was found bent up toward the interface with C_{60} upon deposition of the latter. The observed band bending would assist in suppressing interfacial recombination. In an approach to actively modify this interface by providing stabilizing ligands for the Sn ions of the surface, $FASnI_3$ was treated with the vapor of $2H,2H,3H,3H$-perfluorononanoic acid (FCNA) prior to the deposition of C_{60}, yielding slightly increased PCEs in inverted geometry, however without suppressing iodide migration. These independent findings of highly mobile iodide species within $FASnI_3$ migrating even without application of any external bias strongly indicate that such migration phenomena represent the origin of or at least contribute to the hysteresis described earlier.

Because the interfaces of the absorber layer toward the adjacent ETM and hole-transport material (HTM) represent potentially limiting factors for device performance and because ion migration, dipole formation, and, in general, chemical reactivity have been identified as relevant, a lot of effort was put into optimizing contact formation by the use of alternative ETMs and HTMs or modification of the commonly used materials. Jiang
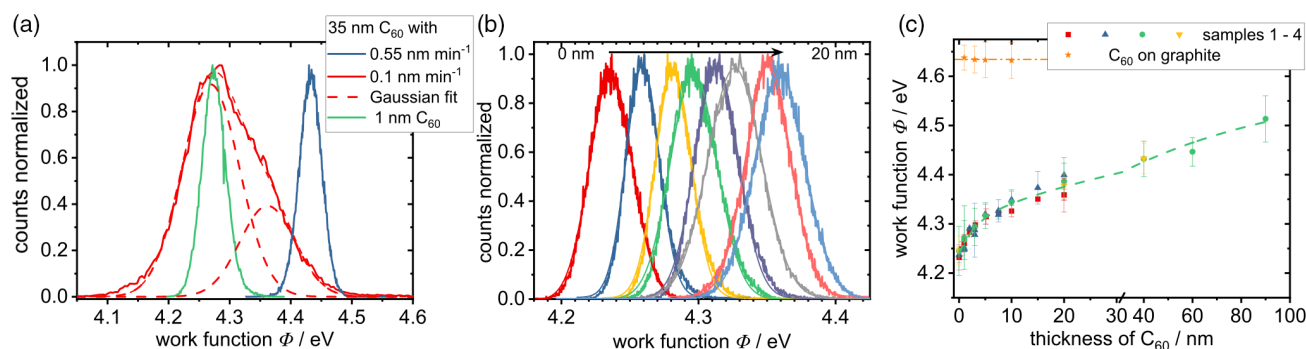

Figure 4. a) Histograms of the work function Φ for 35 nm of C_{60} deposited with different rates on $FASnI_3$ (red and blue). For the small deposition rate, two components can be observed, one of which is attributed to a monolayer of C_{60} (green line), whereas the other corresponds to agglomerates of C_{60}. b) Histograms of the work function obtained for increasing thickness of C_{60} (0–20 nm, indicated by the arrow) deposited on $FASnI_3$. c) Φ as a function of C_{60} deposited on $FASnI_3$ and on graphite (orange line). a–c) Reproduced with permission.[75] Copyright 2020, Springer Nature.
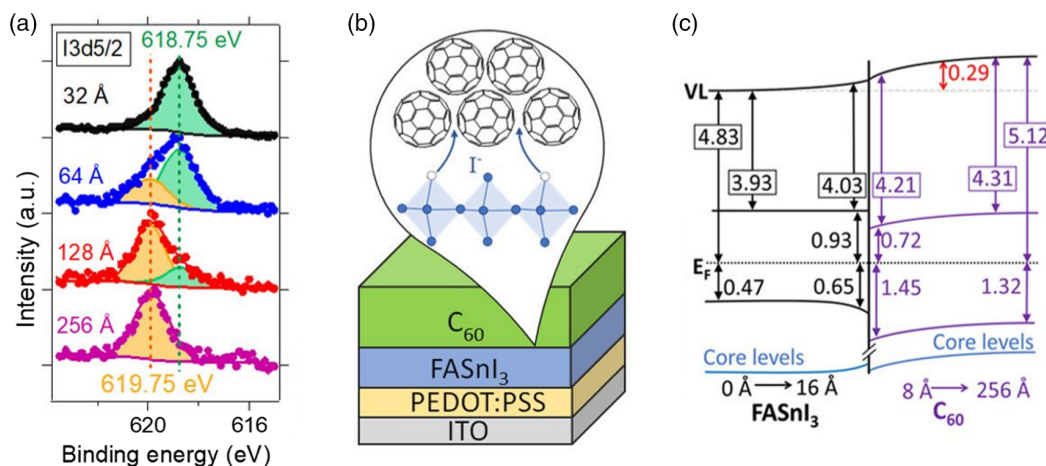
Figure 5. a) XPS iodide signal for different C_{60} film thicknesses during deposition on $FASnI_3$, confirming the presence of iodide in C_{60} stemming from underlying $FASnI_3$. b) Schematics of the sample under investigation and the iodide migration into C_{60}. c) Energy-level alignment of the interface as concluded from a combined ultraviolet photoelectron spectroscopy (UPS) and XPS study. a–c) Reproduced with permission.[76] Copyright 2019, American Chemical Society.

et al. identified the solution-processable C_{60} derivative [6,6]-phyl-C_{61}-butyric acid methyl ester (PCBM) as one reason for the rather low V_{OC} in tin-based PSCs and introduced an indene-C_{60} bisadduct (ICBA) as a valuable alternative (**Figure 6**). The impressively increased V_{oc} of 0.94 V was measured (Figure 6b), which is not only the highest reported so far for tin-based PSCs but it also boosted the PCE to 12.4%, representing a new record for lead-free PSCs at that time.[77] This was explained by the higher LUMO level of ICBA compared to PCBM (Figure 6a), decreasing the energy offset between the perovskite and ETM. This energy difference was confirmed by KPFM measurements across the phase boundary between the perovskite and ETM to obtain the surface potential of both layers, yielding a difference of 20 mV for ICBA in contrast to 100 mV for PCBM (Figure 6c). In addition, the aforementioned iodide migration into the ETM and the consequently increased charge carrier concentration at the interface due to ETM doping by iodide is expected to be less severe for ICBA due to the higher LUMO energy, which suppresses electron injection from the migrated iodide. Such decreased charge density

at the interface obviously led to a suppression of interfacial recombination (Figure 6c), which was, further, confirmed by the strongly increased electroluminescence for the perovskite in contact with ICBA compared with the contact to PCBM.[77]

A similar approach was followed by Ran et al., however focusing on an increase of the work function of the commonly used HTM PEDOT:PSS and, therefore, improved energy-level alignment with $FASnI_3$. It was shown that the thermal deposition of 5 nm of LiF before spin coating of PEDOT:PSS increased the work function of the latter by 70 meV (measured by PES) and consequently increased the V_{OC} of the PSC by 90 mV.[78] The increase of the work function was assigned as caused by a presumably different molecular arrangement of the polymer following the different wettability induced by the thin LiF layer.

Modification of the perovskite interface can also be achieved by surface passivation following perovskite deposition before deposition of the contact phase, as successfully proven by Hayase and co-workers.[79] They applied a solution containing the Lewis base ethane-1,2-diamine (EDA) directly after solution
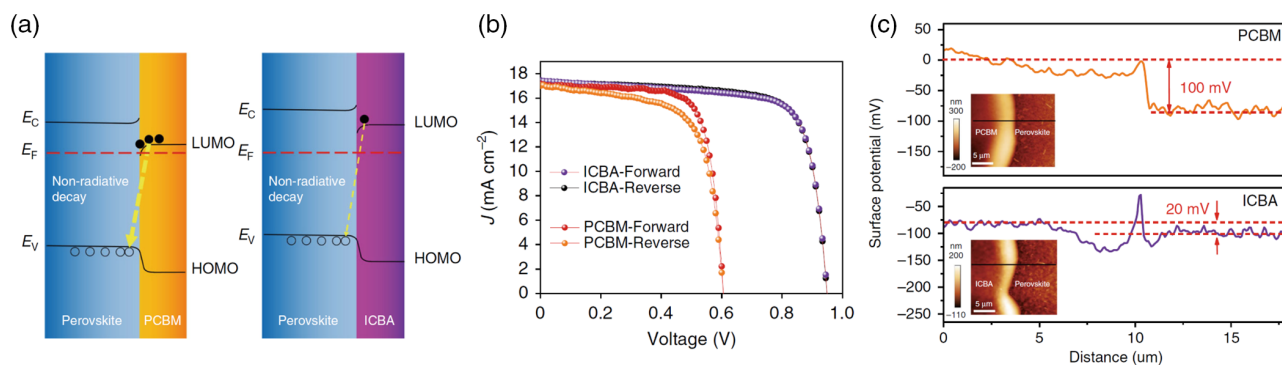

Figure 6. a) Band schematics at the ETM–$FASnI_3$ interface highlighting a decreased nonradiative recombination probability for an optimized energy alignment. b) j–V characteristics of PSCs using ICBA and PCBM, with the former showing suppressed j–V hysteresis and increased V_{OC} and PCE. c) Surface potential resulting from KPFM obtained across the boundary of PCBM (top) and ICBA (bottom) deposited on $FASnI_3$ showing the decreased energy offset between the ETM and perovskite by the use of ICBA. a–c) Reproduced under the terms of the CC-BY Creative Commons Attribution 4.0 International license (https://creativecommons.org/licenses/by/4.0).[77] 2020, The Authors, published by Springer Nature.

processing of the mixed 2D/3D tin-based perovskite $FA_{0.98}EDA_{0.02}SnI_3$ and prior to vapor deposition of C_{60}, resulting in a passivation of surface defects and removal of unreacted SnI_2. An increased V_{OC} could be reached, most likely caused by an attenuated recombination via trap states, however at the expense of a reduced j_{SC} presumably caused by an increased series resistance, due to the insulating character of the surface passivating EDA. This assignment was confirmed by a prolonged electron recombination lifetime and even increased charge collection efficiency for the surface-passivated perovskite layers, as measured by intensity-modulated photocurrent and photovoltage spectroscopy (IMPS and IMVS). To gain deeper insight into the interface modification, the elemental composition at the interface was studied by XPS, expecting a smaller fraction of Sn^{4+} to Sn^{2+} for the EDA-treated film, as undesired doping by Sn^{4+} had been regarded as a major reason for the generally low V_{OC} of tin-based PSCs due to increased nonradiative recombination. Surprisingly, the ratio was very similar in both cases, with, however, binding energies of Sn^{4+} significantly shifted toward higher binding energies in the EDA-passivated layer, indicating a reaction of EDA with Sn^{4+}, obviously suppressing its detrimental influence on PSC properties. An additional finding was a significant deficiency of I^- in relation to Sn at the surface (1:1.09 and 1:19, for the reference and passivated film, respectively), which could explain the generally low V_{OC} for Sn-based PSCs because iodide vacancies are expected to strongly enhance nonradiative recombination. The lowered deficiency following surface passivation provided an additional explanation of the increased PCE and electron lifetime before recombination.[79]

As indicated by these dedicated studies of contact formation with tin-based hybrid perovskites, their interfaces are on one hand, prone to degradation and oxidation and thus responsible for limited device stability and on the other hand very decisive for device function and efficiency. Optimization of the contact materials and the energy-level alignment with the perovskite led and further leads to significant improvement of the device (mainly the V_{OC} and FF). Ionic migration, mainly of I^-, can generally occur, even without any external bias applied, but is significantly enhanced for applied bias voltages. This migration modifies the interface in various ways: it leads to a deficiency of iodide at the surface reaching into the bulk of the perovskite layer and to a doping effect of the iodide-accepting layer, e.g., C_{60}. Both of these consequences are responsible for an increased recombination rate within the perovskite and across the interface. As already touched on in the aforementioned surface studies, a number of strategies have evolved to cope with this problem, reaching from the extended use of mixed 2D/3D structures,[67,71,78,80] to substitution of TiO_2 in "regular," noninverted cell architectures by a less reactive oxide, e.g., Nb_2O_5, and beyond, as separately reviewed recently.[69]

3.2. Studies on the Double Perovskite $Cs_2AgBiBr_6$

The double perovskite $Cs_2AgBiBr_6$ is currently being investigated intensively as a possible absorber material in thin-film devices despite its rather low absorption in the visible spectral range caused by an indirect-bandgap transition,[81,82] which results from a mismatch between Ag d and Bi s orbitals[30] and its rather high exciton binding energies.[83,84] The large interest in this material can be explained by improved stability under ambient conditions[84] and reduced toxicity when compared to lead-based perovskites[85] as well as by the impressively long charge carrier lifetimes in $Cs_2AgBiBr_6$ single crystals and thin films.[86,87] Nevertheless, the highest reported PCE of PCSs based on double perovskites as absorbers is as low as 3.1%,[88] and even this is only achieved by combining the double perovskite with a dye sensitizer as an additional absorber, adsorbed on the mesoporous TiO_2, mainly serving as an ETM. Using $Cs_2AgBiBr_6$ as a single absorber, a lower record efficiency of just 2.81% was reported,[89] which is far below that of lead-based PSCs, but also below efficiencies reported for tin-based PSCs. So it remains doubtful whether absorber layers based on double perovskites can provide a vital alternative to established perovskite absorber layers in PSCs. However, because double perovskite layers still represent a relevant subgroup of less toxic perovskite materials, they can be synthesized under less demanding conditions and may become useful in other possible application, such as photodetectors and light emitting diodes.[32,85,90–92] The following paragraphs are dedicated to studies of interfacing $Cs_2AgBiBr_6$ with optional contact materials in heterojunctions.

3.2.1. Hysteresis in $Cs_2AgBiBr_6$ PSCs

Already in the first reports of $Cs_2AgBiBr_6$ PSCs, j–V hysteresis was reported (**Figure 7**a) and attributed to trapping and detrapping of electrons or holes in defect states and to consequences of ionic migration, reasonably argued for based on a similar crystal structure as the lead-based materials, without, however, specific proof for such a hypothesis.[93] Several subsequent studies, however, showed that PSCs based on $Cs_2AgBiBr_6$ can also be prepared in a way leading to cells that show considerably less hysteresis.[83,94–96]

Yang and co-workers reported that the preparation conditions (e.g., vapor-deposited vs solution-processed) strongly influence the degree of j–V hysteresis. They attributed this observation to the slightly different stoichiometries in the films depending on the preparation conditions, yielding a more efficient charge extraction at the interfaces for solution-processed films.[94] A similar shape of hysteresis for fully vapor-deposited double perovskite films was reported by Wang et al. and attributed to nonideal charge extraction at the contacts.[97] Longo et al. investigated PSCs using PVD-deposited $Cs_2AgBiBr_6$ with varying thicknesses and also found j–V characteristics that strongly depended on the scan direction—without finding a clear correlation on the absorber thickness. In contrast to previous reports, they found the V_{OC} to be strongly affected by the hysteresis in a similar way to that found earlier for mixed MA/FA tin-based PSCs (Figure 3c) rather than the FF, as usually reported. This finding pointed toward a different origin of the hysteresis in V_{OC} depending on the scan direction as opposed to that in the FF. As a rather low electron-diffusion length was reported as the limiting factor in these PSCs as opposed to a considerably larger hole-diffusion length,[98] one could argue that an unbalanced charge transport within the absorber layer depending on scan direction might lead to unsymmetric charge accumulation and, therefore, differences in V_{OC}. Pantaler et al. reported that the degree of hysteresis in PSCs with double perovskites strongly depended on the choice of HTM. Whereas the
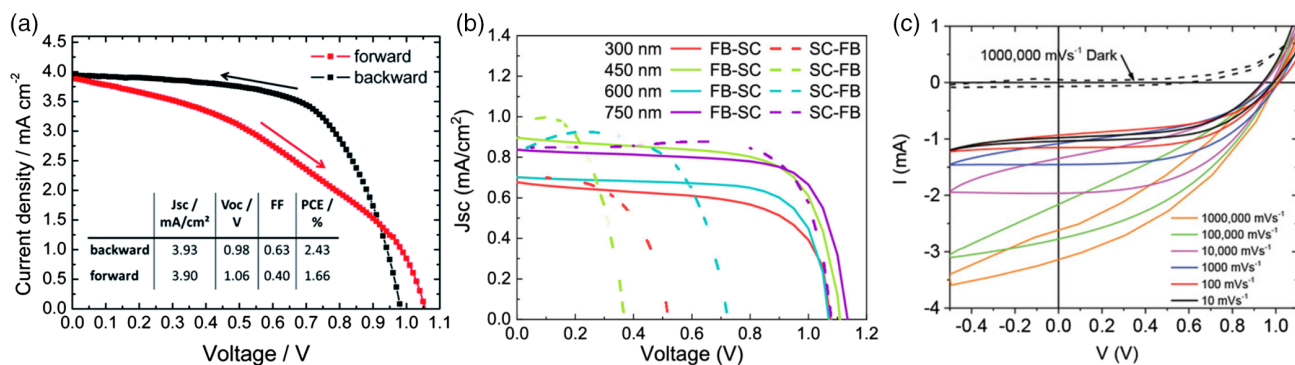
Figure 7. a) *j–V* characteristics of a PSC based on spin-coated Cs$_2$AgBiBr$_6$ showing large discrepancy between forward and backward scan. b) *j–V* curves (forward scan: solid lines, reverse scan: dashed lines) of vapor-deposited Cs$_2$AgBibr$_6$-based PSCs with varying absorber layer thickness. c) *I–V* loops of PSCs based on solution-grown Cs$_2$AgBiBr$_6$ with different scan rates starting at 1.1 V after application of 1.1 V for 10 s. a) Reproduced with permission.[93] Copyright 2017, Royal Society of Chemistry. b) Reproduced with permission.[98] Copyright 2020, American Chemical Society. c) Reproduced with permission.[99] Copyright 2021, Wiley-VCH.

commonly used 2,2′,7,7′-tetrakis[*N,N*-di-(4-methoxyphenyl)amino]-9,9′-spirobifluorene (spiro-OMeTAD) led to *j–V* hysteresis in cell characteristics, poly-[bis-(4-phenyl)-(2,4,6-trimethyl-phenyl)-amin] (PTAA) did not. An identification of the mechanistic reason for the improvement has not been provided yet.[96] Such a difference between these HTMs indicates the relevance of interfaces for the mechanism behind the hysteresis in PSCs depending on scan direction. The interface to the ETM also showed an influence on the observed hysteresis, which could be reduced by increased film quality of the deposited double perovskite leading to a reduced electron trap density in the absorber layer when the latter is prepared on appropriately doped TiO$_2$.[89]

A systematic study by Tress and co-workers aimed at the origin of the generally measured *j–V* hysteresis and reasons for the low efficiencies typically observed in PSCs based on double perovskites. They systematically studied cell characteristics under variation of cell architecture, scan rate, and scan direction.[99] P3HT or spiro-OMeTAD were used as HTM, and planar or mesoporous (mp) TiO$_2$ was used as ETM. The choice of HTM and ETM was identified as the main factor that influenced the hysteresis. Cells with P3HT as HTM and mp-TiO$_2$ as ETM showed almost no hysteresis even for high scan rates, in contrast to strongly the increased hysteresis for PSCs using spiro-OMeTAD as the HTM, irrespective of the ETM used, confirming the results of Pantaler et al., obtained by comparing PTAA with spiro-OMeTAD. Further, the hysteresis was strongly influenced by the scan rate, with higher rates leading to an increased difference between reverse and forward scan, whereas lower rates (0.1 V s^{-1}) showed negligible hysteresis. Therefore, they strongly recommended to report scan properties along with PSC data and argued in favor of a standard characterization protocol, as established for lead-based PSCs.[47,100–102] In addition, *j–V* scans after prebiasing at V_{OC} for 10 s were performed and resulted in strongly increased j_{SC} for high scan rates (Figure 7c). By combining their findings about the choice of the contact material, scan rate, and pre-biasing dependence, they concluded that the migration of ions in Cs$_2$AgBiBr$_6$ is influenced by the external bias, which yields a modification of the built-in potential in the absorber. Ions are expected to move rather slowly and, therefore, their concentration could not equilibrate upon rapid changes of bias voltage as

occurring in fast scans and were held responsible for the large impact of the scan rate on hysteresis. Such a bias-induced change of ion concentration in the absorber and at the contacts affected the collection efficiency at the interfaces and, thus, was found to strongly influence j_{SC} with minor effects on V_{OC} and FF.[99]

Ghasemi et al. investigated details of ion diffusion from Cs$_2$AgBiBr$_6$ into the HTM and metal electrodes after ambient storage for 68 days to improve the understanding of possible device degradation mechanisms. By optimization of the cell geometry, they identified a combination of P3HT as HTM and copper as low-cost metal back contact as ideal and achieved a reasonable PCE of 1.91%.[103] A focused ion beam was used to prepare cross-sections of devices before and after storage and these were analyzed with respect to the elemental distribution across the different layers using transmission electron microscopy. Diffusion of Ag$^+$ and Br$^-$ from the double perovskite through P3HT toward the metal contact was observed. This finding was confirmed by XPS depth profiling on freshly prepared and degraded devices and, thus, ion migration was identified as part of a possible degradation mechanism. The energy barrier for ion movement was calculated to be significantly smaller for Ag$^+$ and Br$^-$ than for Cs$^+$ or Bi^{3+} and explains the experimental findings.[103] As their experiments aimed at understanding ion diffusion and degradation over a long period, hysteresis was not investigated. However, because the migration of mobile ions, namely, Ag$^+$ and Br$^-$, was demonstrated, one might expect these to move under the influence of external bias, which supports the claims made by Tress and co-workers that the dependence of hysteresis on scan rate and cell characteristics is governed by such mobile ions. Despite these studies on ionic motion and its effects on solar cell properties, a detailed understanding of this material under the influence of external electric fields and a direct correlation of ionic migration with changes in the energy-level alignment with HTMs and EMTs is still missing.

3.2.2. Interface Modification and Energy-Level Alignment in Contacts to Cs$_2$AgBiBr$_6$

Several groups successfully tried to improve the function of double-perovskite PSCs by choosing appropriate charge-selective

ADVANCED
SCIENCE NEWS

www.advancedsciencenews.com

physica **pssrrrl**
status
solidi

www.pss-rapid.com

layers, often but not always in parallel to attempts to understand or suppress hysteresis, as discussed earlier. At the HTM side, the frequently used spiro-OMeTAD was proven to not be an ideal contact material since improved PCE was achieved by replacing it with PTAA[96] or poly[(5-fluoro-2,1,3-benzothiadiazole-4,7-diyl)(4,4-dihexadecyl-4H-cyclopenta[2,1-b:3,4-b′]dithiophene-2,6-diyl)(6-fluoro-2,1,3-benzothiadiazole-4,7-diyl)(4,4-dihexadecyl-4H-cyclopenta[2,1-b:3,4-b′]dithiophene-2,6-diyl)] (PCDTFBT).[104] When PTAA was used instead of spiro-OMeTAD, an increase in V_{OC} and FF was observed at, however, a reduced j_{SC}. The observed large differences cannot be explained by differences in the energy levels of the materials because these are very similar for spiro-OMeTAD and PTAA.[96] However, interfacial reactions and ion transfer between the materials (as observed, e.g., for I^- in the contact $FASnI_3/C_{60}$) have not been investigated yet but may occur for these materials as well and influence charge transfer and recombination at the interface of HTMs with $Cs_2AgBiBr_6$, because mobile ions were found in $Cs_2AgBiBr_6$. Therefore, similar studies as described earlier for $FASnI_3$ would be desirable also for contacts to $Cs_2AgBiBr_6$ to achieve a better understanding of the energy-level alignment.

In a recent study, ETM and HTM contacts to $Cs_2AgBiBr_6$ were optimized with beneficial effect on V_{OC} and j_{SC}. Luo et al. modified the surface of TiO_2 by spin coating a thin layer of C_{60}, which led to improved crystallization of the subsequently spin-coated double perovskite shown by the increased grain size and reduced roughness (**Figure 8**c).[104] Improved charge transfer across that interface was found and revealed a reduced trap density and improved electron mobility in the double perovskite layer, attributed to an optimized film thickness and energy-level alignment (Figure 8a). Replacement of spiro-OMeTAD as the HTM by PCDTFBT yielded a higher PCE (Figure 8b), which was due to the improved energy-level alignment and increased hole mobility in PCDTFBT. Increased recombination resistance (R_{rec}) and reduced series resistance of the cell with optimized contacts were obtained by impedance spectroscopy, which confirmed the findings of improved charge transport across the interface and increased mobility of charge carriers in the HTM.[104]

To compensate for the rather low light-harvesting efficiency of $Cs_2AgBiBr_6$, a modification of the interface by means of a

light-absorbing (sensitizer) dye was recently suggested almost simultaneously by two different groups.[105,106] Wang and co-workers substituted the commonly used HTMs by zinc dodecyl 3-hydroxymethylpyropheophorbide-a (Zn-Chl) and found not only an enhanced charge-extraction ability for this new HTM when compared to PTAA or spiro-OMeTAD, but also a spectrally extended EQE due to the sensitization by Zn-Chl, contributing to the j_{SC} (**Figure 9**a,b). The cell using Zn-Chl as the HTM, however, showed severe hysteresis with reduced V_{OC} and FF for the forward scan (Figure 9c), which was attributed to trapping and detrapping effects without, however, discussing the role of Zn-Chl.[106] Yang et al. improved the optical absorption of $Cs_2AgBiBr_6$ cells by depositing a thin layer of the ruthenium dye N719, well established as a sensitizer in (solid-state) dye-sensitized solar cells (DSSCs)[107] but also as a cosensitizer in quantum dot solar cells,[108] on top of the double perovskite, as shown by the SEM cross-section in Figure 9e. In addition to the beneficial effect on j_{SC}, increased V_{OC} was found for the dye-sensitized cell compared to the reference cell (Figure 9d).[105] Similar to Wang et al., they attributed these enhancements not only to the increased EQE caused by the additional absorption of the dye, but also to an improved energy-level alignment at the interface between $Cs_2AgBiBr_6$ and spiro-OMeTAD due to the dye interlayer (as measured by PES), facilitating hole extraction at that interface (Figure 9f). Impedance analysis revealed a significantly increased recombination resistance R_{rec} for the cell incorporating the dye interlayer, which was interpreted as a reduced interfacial recombination rate reached by the passivation of surface defects. Such a reduced recombination rate was confirmed by light-intensity-dependent V_{OC} measurements because the ideality factor was found considerably decreased for the cell with the dye interlayer. A combination of these effects was suggested to yield an improved V_{OC}, which, in combination with the increased j_{SC} as a consequence of improved absorption, led to the impressive PCE of 2.84%.[105] The work on the use of Zn-Chl as HTM was extended by the sensitization of TiO_2 with methyl *trans*-32-carboxy-pyropheophorbide-a (C-Chl) prior to the deposition of $Cs_2AgBiBr_6$[88] and spiro-OMeTAD as HTM (**Figure 10**a) to yield the record PCE of 3.11%, comprising an increase of j_{SC} (as expected by
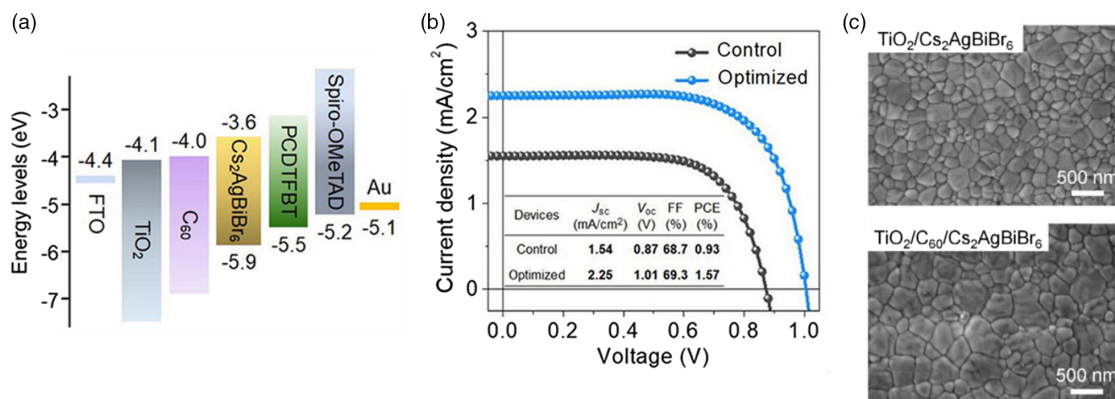

Figure 8. a) Energy levels of all layers in PSCs based on $Cs_2AgBiBr_6$ showing improved alignment for the use of C_{60} and PCDTFBT. b) j–V characteristics of the best-performing cell compared to the reference cell with spiro-OMeTAD and without C_{60}. c) Scanning electron microscopy images of $Cs_2AgBiBr_6$ deposited on TiO_2 without (top) and with a thin interlayer of C_{60}. a–c) Reproduced with permission.[104] Copyright 2021, Elsevier Inc.
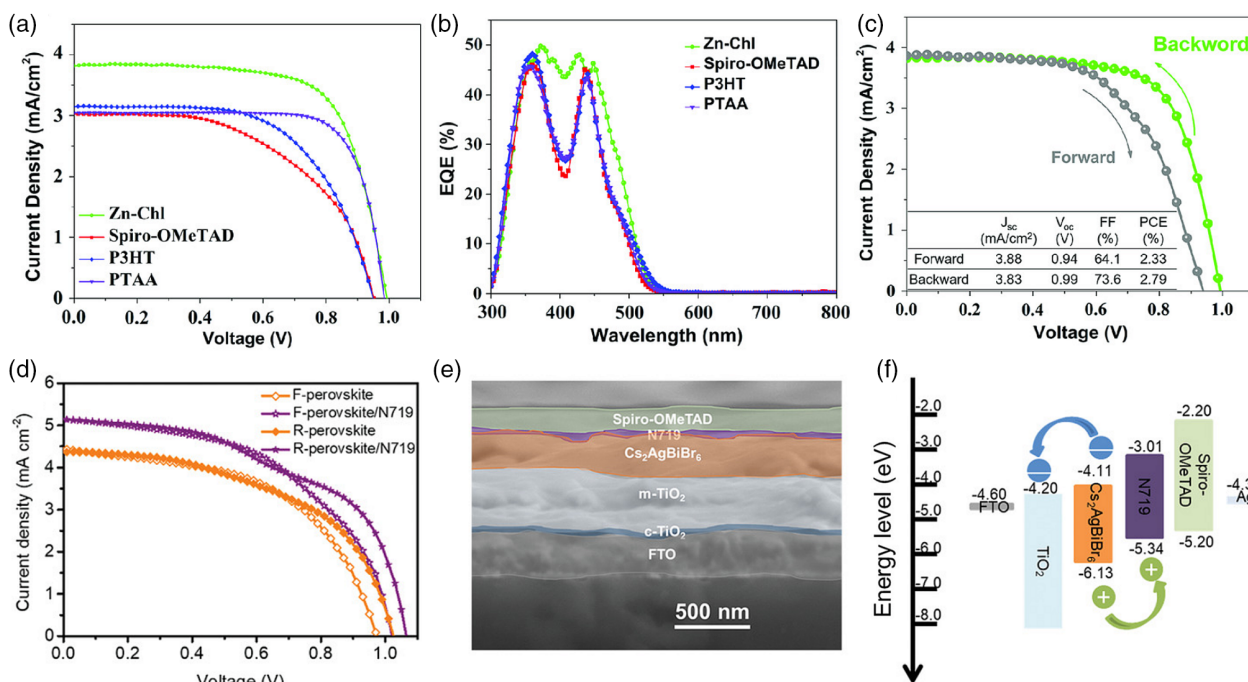
Figure 9. a) j–V characteristics for $Cs_2AgBiBr_6$-based PSCs using different HTMs. b) Comparison of the external quantum efficiency (EQE) for the PSCs using different HTMs. c) Hysteresis for a $Cs_2AgBiBr_6$-based PSC using Zn-Chl as the HTM. d) Forward and reverse j–V scans for a $Cs_2AgBiBr_6$ PSC with and without an N719 interlayer. e) SEM of a cross-section of such a solar cell including a N719 interlayer. f) Energy-level alignment of the materials used in a $Cs_2AgBiBr_6$ PSC including an N719 interlayer. a–c) Reproduced with permission.[106] Copyright 2020, Wiley-VCH. d–f) Reproduced with permission.[105] Copyright 2020, Wiley-VCH.

optimized absorption/EQE, Figure 10b,c) and, further, considerably improved V_{OC}, FF, and reduced hysteresis. A decreased ideality factor and a faster decay of photoluminescence led to the conclusion that interfacial nonradiative recombination was suppressed whereas electron extraction was facilitated at the ETM/C-Chl/$Cs_2AgBiBr_6$ interface. The resistance obtained by impedance spectroscopy was decreased, which was interpreted as improved charge transfer at the interface. This interpretation, however, seems to include a certain contradiction to the aforementioned work by Yang et al.,[105] Luo et al.,[104] and to their own previous work,[106] in which an increase of this resistance by the dye

interlayer was reported and interpreted as beneficial because it was assigned to an increased recombination resistance.

Despite increased PCEs achieved by combining $Cs_2AgBiBr_6$ with dyes either adsorbed on the mesoporous TiO_2 scaffold or as HTM, the efficiencies reached are far from competing with DSSCs using the same sensitizer, e.g., 10.1% with N719 combined with $CsSnI_3$ as solid-state HTM,[107] higher even than the spectroscopically limited maximum efficiency of 7.92% for pure $Cs_2AgBiBr_6$ cells.[82] Given the fact that the dye-sensitized mesoporous layer in these DSSCs is larger in thickness by an order of magnitude compared to the previously described
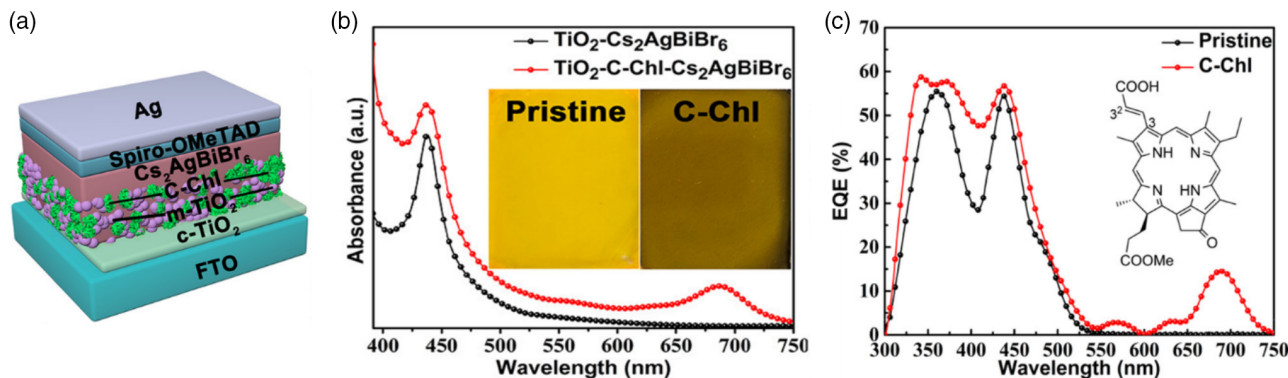

Figure 10. a) Schematics of $Cs_2AgBiBr_6$-based PSCs comprising a dye-sensitized mp-TiO_2 layer. b) Photographs and UV–vis absorption spectrum of the absorber layer with and without dye sensitization. c) EQE spectrum showing the contribution of the improved absorption spectrum. a–c) Reproduced with permission.[88] Copyright 2021, American Chemical Society.

PSCs, the limited contribution of dyes to the EQE in PSCs is not surprising. Therefore, to compete either with the efficiencies of DSSCs or with those of lead- or tin-based PSCs, the absorbing properties of the double perovskites need to be enhanced, e.g., by partially or fully substituting $Bi^{3+[109–112]}$ or Ag^{+}.[113] Nevertheless, it remains debatable whether such double perovskites are indeed suitable as absorber materials in PSCs. However, the materials certainly have proven to be interesting from a fundamental semiconductor physics point of view, carry the big advantage of little toxicity and high chemical stability even under ambient conditions, and might, therefore, be useful for other upcoming optoelectronic applications, e.g., as photo- or X-ray detectors[114] or in devices based on their luminescence.[112]

4. Conclusion

The two main groups of materials that are discussed as possible alternatives to lead-based perovskites in the already quite well-established photovoltaic cells carry a number of common features with each other and with their lead counterparts, but also some significant differences. Some of these parameters are based on the physics of the materials, but others lie in a significant difference in the level of knowledge. Despite the different composition of both described materials—the inorganic double perovskite incorporating bromide as anion and the hybrid organic–inorganic tin perovskite with iodide as anion—the mechanisms and challenges are comparable up to a certain degree and the level of knowledge is still low for both groups of materials when compared to the well-established lead halide perovskites. The energy-level alignment was identified as critical for both tin perovskites and double perovskites to improve the performance of devices to any competitive level. For the tin-based compounds, a lot more effort already has been invested into understanding the interaction of the perovskite with the contacts, which yielded a significantly improved understanding of ion diffusion inside the material and in interfaces with contact layers, with a clear impact on charge transport and band bending within the contacts. The work on double perovskites in this respect has just started. Hysteresis in the current–voltage characteristics has been reported for both materials as it was apparent in reports on PSCs based on lead-based perovskites—with similar explanation models valid because all these metal halide perovskite structures seem to be prone to ion migration and often seem to contain a rather high concentration of (shallow) defects, which can act as trap states for (photogenerated) charge carriers but which also seem to play a relevant role in ion migration. For tin-based PSCs, therefore, quite some progress has been made and they presently represent the most promising alternative to lead-based PSCs despite inherently lower efficiencies. However, for $Cs_2AgBiBr_6$ hysteresis phenomena are not very well understood yet, which is due to the very narrow database on the ion-migrating properties in double perovskites, as well as on contact formation with established and, possibly, new HTMs. An increasing number of recent studies in this field, however, showed that the contacts appear to be a major contributor to hysteresis, recombination, and series resistance and, therefore, their analysis and optimization hold good promise for the further development of devices based on these materials.

Conflict of Interest

The authors declare no conflict of interest.

[1] O. Edenhofer, R. Pichs Madruga, Y. Sokona, *Renewable Energy Sources and Climate Change Mitigation*, Cambridge University Press, New York **2012**.

[2] Frankfurt School-UNEP Centre/BNEF, **2019**.

[3] Frankfurt School-UNEP Centre/BNEF, **2020**.

[4] M. Green, *Third Generation Photovoltaics*, Springer, Berlin/Heidelberg, Germany **2006**.

[5] A. Kojima, K. Teshima, Y. Shirai, T. Miyasaka, *J. Am. Chem. Soc.* **2009**, *131*, 6050.

[6] NREL, Best Research-Cell Efficiency Chart, https://www.nrel.gov/pv/assets/pdfs/best-research-cell-efficiencies.20200406.pdf, (accessed: July 2021).

[7] T. Ibn-Mohammed, S.C.L. Koh, I. M. Reaney, A. Acquaye, G. Schileo, K. B. Mustapha, R. Greenough, *Renewable Sustainable Energy Rev.* **2017**, *80*, 1321.

[8] J. Gong, S. B. Darling, F. You, *Energy Environ. Sci.* **2015**, *8*, 1953.

[9] I. Celik, Z. Song, A. J. Cimaroli, Y. Yan, M. J. Heben, D. Apul, *Sol. Energy Mater. Sol. Cells* **2016**, *156*, 157.

[10] C. Wadia, A. P. Alivisatos, D. M. Kammen, *Environ. Sci. Technol.* **2009**, *43*, 2072.

[11] N. Li, X. Niu, Q. Chen, H. Zhou, *Chem. Soc. Rev.* **2020**, *49*, 8235.

[12] Y. Rong, Y. Hu, A. Mei, H. Tan, M. I. Saidaminov, S. I. Seok, M. D. McGehee, E. H. Sargent, H. Han, *Science* **2018**, *361*, eaat8235.

[13] Y. Y. Kim, T.-Y. Yang, R. Suhonen, A. Kemppainen, K. Hwang, N. J. Jeon, J. Seo, *Nat. Commun.* **2020**, *11*, 5146.

[14] A. Babayigit, A. Ethirajan, M. Muller, B. Conings, *Nat. Mater.* **2016**, *15*, 247.

[15] K. P. Goetz, A. D. Taylor, Y. J. Hofstetter, Y. Vaynzof, *ACS Appl. Mater. Interfaces* **2021**, *13*, 1.

[16] J. Li, H.-L. Cao, W.-B. Jiao, Q. Wang, M. Wei, I. Cantone, J. Lü, A. Abate, *Nat. Commun.* **2020**, *11*, 310.

[17] A. Abate, *Joule* **2017**, *1*, 659.

[18] C. C. Stoumpos, C. D. Malliakas, M. G. Kanatzidis, *Inorg. Chem.* **2013**, *52*, 9019.

[19] G. C. Papavassiliou, *Prog. Solid State Chem.* **1997**, *25*, 125.

[20] Y. Takahashi, H. Hasegawa, Y. Takahashi, T. Inabe, *J. Solid State Chem.* **2013**, *205*, 39.

[21] L. Lanzetta, T. Webb, N. Zibouche, X. Liang, D. Ding, G. Min, R. J. E. Westbrook, B. Gaggio, T. J. Macdonald, M. S. Islam, S. A. Haque, *Nat. Commun.* **2021**, *12*, 2853.

[22] L. Ma, F. Hao, C. C. Stoumpos, B. T. Phelan, M. R. Wasielewski, M. G. Kanatzidis, *J. Am. Chem. Soc.* **2016**, *138*, 14750.

[23] T. Handa, A. Wakamiya, Y. Kanemitsu, *APL Mater.* **2019**, *7*, 80903.

[24] R. L. Milot, M. T. Klug, C. L. Davies, Z. Wang, H. Kraus, H. J. Snaith, M. B. Johnston, L. M. Herz, *Adv. Mater.* **2018**, *30*, e1804506.

[25] F. Hao, C. C. Stoumpos, D. H. Cao, R. P. H. Chang, M. G. Kanatzidis, *Nat. Photonics* **2014**, *8*, 489.

[26] W.-F. Yang, J.-J. Cao, C. Dong, M. Li, Q.-S. Tian, Z.-K. Wang, L.-S. Liao, *Appl. Phys. Lett.* **2021**, *118*, 23501.

[27] X. Jiang, H. Li, Q. Zhou, Q. Wei, M. Wei, L. Jiang, Z. Wang, Z. Peng, F. Wang, Z. Zang, K. Xu, Y. Hou, S. Teale, W. Zhou, R. Si, X. Gao, E. H. Sargent, Z. Ning, *J. Am. Chem. Soc.* **2021**, *143*, 10970.

[28] K. Nishimura, M. A. Kamarudin, D. Hirotani, K. Hamada, Q. Shen, S. Iikubo, T. Minemoto, K. Yoshino, S. Hayase, *Nano Energy.* **2020**, *74*, 104858.

[29] E. T. McClure, M. R. Ball, W. Windl, P. M. Woodward, *Chem. Mater.* **2016**, *28*, 1348.

[30] A. H. Slavney, T. Hu, A. M. Lindenberg, H. I. Karunadasa, *J. Am. Chem. Soc.* **2016**, *138*, 2138.

[31] B. Yang, X. Mao, F. Hong, W. Meng, Y. Tang, X. Xia, S. Yang, W. Deng, K. Han, *J. Am. Chem. Soc.* **2018**, *140*, 17001.

[32] P.-K. Kung, M.-H. Li, P.-Y. Lin, J.-Y. Jhang, M. Pantaler, D. C. Lupascu, G. Grancini, P. Chen, *Sol. RRL* **2020**, *4*, 1900306.

[33] S. Shao, M. A. Loi, *Adv. Mater. Interfaces* **2020**, *7*, 1901469.

[34] P. Schulz, D. Cahen, A. Kahn, *Chem. Rev.* **2019**, *119*, 3349.

[35] J. M. Frost, A. Walsh, *Acc. Chem. Res.* **2016**, *49*, 528.

[36] T.-Y. Yang, G. Gregori, N. Pellet, M. Grätzel, J. Maier, *Angew. Chem. Int. Ed.* **2015**, *54*, 7905.

[37] M. Stumpp, R. Ruess, J. Horn, J. Tinz, D. Schlettwein, *Phys. Status Solidi A.* **2016**, *213*, 38.

[38] Y. Yuan, T. Li, Q. Wang, J. Xing, A. Gruverman, J. Huang, *Sci. Adv.* **2017**, *3*, e1602164.

[39] A. Gómez, Q. Wang, A. R. Goñi, M. Campoy-Quiles, A. Abate, *Energy Environ. Sci.* **2020**, *13*, 1892.

[40] A. Colsmann, T. Leonhard, A. D. Schulz, H. Röhm, *Energy Environ. Sci.* **2020**, *13*, 1888.

[41] A. Gómez, Q. Wang, A. R. Goñi, M. Campoy-Quiles, A. Abate, *Energy Environ. Sci.* **2019**, *12*, 2537.

[42] H. Röhm, T. Leonhard, M. J. Hoffmann, A. Colsmann, *Energy Environ. Sci.* **2017**, *10*, 950.

[43] H. Röhm, T. Leonhard, A. D. Schulz, S. Wagner, M. J. Hoffmann, A. Colsmann, *Adv. Mater.* **2019**, *31*, e1806661.

[44] R. Singh, M. Parashar, in *Soft-Matter Thin Film Solar Cells*, AIP Publishing Books, Melville, NY **2020**, pp. 1–42.

[45] D.-H. Kang, N.-G. Park, *Adv. Mater.* **2019**, *31*, e1805214.

[46] P. Liu, W. Wang, S. Liu, H. Yang, Z. Shao, *Adv. Energy Mater.* **2019**, *9*, 1803017.

[47] E. L. Unger, A. Czudek, H.-S. Kim, W. Tress, in *Characterization Techniques for Perovskite Solar Cell Materials*, Elsevier, Amsterdam, The Netherlands **2020**, pp. 81–108.

[48] M. Stumpp, R. Ruess, J. Müßener, D. Schlettwein, *Mater. Today Chem.* **2017**, *4*, 97.

[49] W. Tress, N. Marinova, T. Moehl, S. M. Zakeeruddin, M. K. Nazeeruddin, M. Grätzel, *Energy Environ. Sci.* **2015**, *8*, 995.

[50] A. Bou, A. Pockett, D. Raptis, T. Watson, M. J. Carnie, J. Bisquert, *J. Phys. Chem. Lett.* **2020**, 8654.

[51] E. Ghahremanirad, A. Bou, S. Olyaee, J. Bisquert, *J. Phys. Chem. Lett.* **2017**, *8*, 1402.

[52] T. Noma, D. Taguchi, T. Manaka, M. Iwamoto, *Mol. Crystals Liquid Crystals* **2019**, *686*, 92.

[53] B. Philippe, M. Saliba, J.-P. Correa-Baena, U. B. Cappel, S.-H. Turren-Cruz, M. Grätzel, A. Hagfeldt, H. Rensmo, *Chem. Mater.* **2017**, *29*, 3589.

[54] B. Philippe, B.-W. Park, R. Lindblad, J. Oscarsson, S. Ahmadi, E. M. J. Johansson, H. Rensmo, *Chem. Mater.* **2015**, *27*, 1720.

[55] S. Tao, I. Schmidt, G. Brocks, J. Jiang, I. Tranca, K. Meerholz, S. Olthof, *Nat. Commun.* **2019**, *10*, 2560.

[56] P. Schulz, L. L. Whittaker-Brooks, B. A. MacLeod, D. C. Olson, Y.-L. Loo, A. Kahn, *Adv. Mater. Interfaces* **2015**, *2*, 1400532.

[57] Q.-K. Wang, R.-B. Wang, P.-F. Shen, C. Li, Y.-Q. Li, L.-J. Liu, S. Duhm, J.-X. Tang, *Adv. Mater. Interfaces* **2015**, *2*, 1400528.

[58] W. Melitz, J. Shen, A. C. Kummel, S. Lee, *Surf. Sci. Rep.* **2011**, *66*, 1.

[59] S. Chen, X. Wen, J. S. Yun, S. Huang, M. Green, N. J. Jeon, W. S. Yang, J. H. Noh, J. Seo, S. I. Seok, A. Ho-Baillie, *ACS Appl. Mater. Interfaces* **2017**, *9*, 6072.

[60] V. W. Bergmann, S. A. L. Weber, F. Javier Ramos, M. K. Nazeeruddin, M. Grätzel, D. Li, A. L. Domanski, I. Lieberwirth, S. Ahmad, R. Berger, *Nat. Commun.* **2014**, *5*, 5001.

[61] C.-S. Jiang, M. Yang, Y. Zhou, B. To, S. U. Nanayakkara, J. M. Luther, W. Zhou, J. J. Berry, J. van de Lagemaat, N. P. Padture, K. Zhu, M. M. Al-Jassim, *Nat. Commun.* **2015**, *6*, 8397.

[62] S. A. L. Weber, I. M. Hermes, S.-H. Turren-Cruz, C. Gort, V. W. Bergmann, L. Gilson, A. Hagfeldt, M. Graetzel, W. Tress, R. Berger, *Energy Environ. Sci.* **2018**, *11*, 2404.

[63] S. T. Birkhold, J. T. Precht, H. Liu, R. Giridharagopal, G. E. Eperon, L. Schmidt-Mende, X. Li, D. S. Ginger, *ACS Energy Lett.* **2018**, *3*, 1279.

[64] Z. Kang, H. Si, M. Shi, C. Xu, W. Fan, S. Ma, A. Kausar, Q. Liao, Z. Zhang, Y. Zhang, *Sci. China Mater.* **2019**, *62*, 776.

[65] Z. Xiao, Y. Yuan, Y. Shao, Q. Wang, Q. Dong, C. Bi, P. Sharma, A. Gruverman, J. Huang, *Nat. Mater.* **2015**, *14*, 193.

[66] T. Noma, D. Taguchi, T. Manaka, M. Iwamoto, *J. Appl. Phys.* **2018**, *124*, 175501.

[67] J. Horn, M. Scholz, K. Oum, T. Lenzer, D. Schlettwein, *APL Mater.* **2019**, *7*, 31112.

[68] G. Grancini, M. K. Nazeeruddin, *Nat. Rev. Mater.* **2019**, *4*, 4.

[69] Z. Wan, H. Lai, S. Ren, R. He, Y. Jiang, J. Luo, Q. Chen, X. Hao, Y. Wang, J. Zhang, L. Wu, D. Zhao, *J. Energy Chem.* **2021**, *57*, 147.

[70] G. Grancini, C. Roldán-Carmona, I. Zimmermann, E. Mosconi, X. Lee, D. Martineau, S. Narbey, F. Oswald, F. de Angelis, M. Grätzel, M. K. Nazeeruddin, *Nat. Commun.* **2017**, *8*, 15684.

[71] S. Shao, J. Liu, G. Portale, H.-H. Fang, G. R. Blake, G. H. ten Brink, L. J. A. Koster, M. A. Loi, *Adv. Energy Mater.* **2017**, *7*, 1702019.

[72] D. S. Lee, J. S. Yun, J. Kim, A. M. Soufiani, S. Chen, Y. Cho, X. Deng, J. Seidel, S. Lim, S. Huang, A. W. Y. Ho-Baillie, *ACS Energy Lett.* **2018**, *3*, 647.

[73] K. Chen, P. Wu, W. Yang, R. Su, D. Luo, X. Yang, Y. Tu, R. Zhu, Q. Gong, *Nano Energy* **2018**, *49*, 411.

[74] B.B. Yu, M. Liao, Y. Zhu, X. Zhang, Z. Du, Z. Jin, Di Liu, Y. Wang, T. Gatti, O. Ageev, Z. He, *Adv. Funct. Mater.* **2020**, *30*, 2002230.

[75] J. Horn, D. Schlettwein, *J. Mater. Res.* **2020**, *35*, 2897.

[76] A. M. Boehm, T. Liu, S. M. Park, A. Abtahi, K. R. Graham, *ACS Appl. Mater. Interfaces* **2020**, *12*, 5209.

[77] X. Jiang, F. Wang, Q. Wei, H. Li, Y. Shang, W. Zhou, C. Wang, P. Cheng, Q. Chen, L. Chen, Z. Ning, *Nat. Commun.* **2020**, *11*, 1245.

[78] C. Ran, J. Xi, W. Gao, F. Yuan, T. Lei, B. Jiao, X. Hou, Z. Wu, *ACS Energy Lett.* **2018**, *3*, 713.

[79] M. A. Kamarudin, D. Hirotani, Z. Wang, K. Hamada, K. Nishimura, Q. Shen, T. Toyoda, S. Iikubo, T. Minemoto, K. Yoshino, S. Hayase, *J. Phys. Chem. Lett.* **2019**, *10*, 5277.

[80] E. Jokar, C.-H. Chien, C.-M. Tsai, A. Fathi, E. W.-G. Diau, *Adv. Mater.* **2019**, *31*, 1804835.

[81] G. Volonakis, M. R. Filip, A. A. Haghighirad, N. Sakai, B. Wenger, H. J. Snaith, F. Giustino, *J. Phys. Chem. Lett.* **2016**, *7*, 1254.

[82] C. N. Savory, A. Walsh, D. O. Scanlon, *ACS Energy Lett.* **2016**, *1*, 949.

[83] R. Kentsch, M. Scholz, J. Horn, D. Schlettwein, K. Oum, T. Lenzer, *J. Phys. Chem. C.* **2018**, *122*, 25940.

[84] C. Wu, Q. Zhang, Y. Liu, W. Luo, X. Guo, Z. Huang, H. Ting, W. Sun, X. Zhong, S. Wei, S. Wang, Z. Chen, L. Xiao, *Adv. Sci.* **2018**, *5*, 1700759.

[85] L. Lu, X. Pan, J. Luo, Z. Sun, *Chem. Eur. J.* **2020**, *26*, 16975.

[86] D. Bartesaghi, A. H. Slavney, M. C. Gélvez-Rueda, B. A. Connor, F. C. Grozema, H. I. Karunadasa, T. J. Savenije, *J. Phys. Chem. C.* **2018**, *122*, 4809.

[87] R. L. Z. Hoye, L. Eyre, F. Wei, F. Brivio, A. Sadhanala, S. Sun, W. Li, K. H. L. Zhang, J. L. MacManus-Driscoll, P. D. Bristowe, R. H. Friend, A. K. Cheetham, F. Deschler, *Adv. Mater. Interfaces* **2018**, *5*, 1800464.

[88] B. Wang, N. Li, L. Yang, C. Dall'Agnese, A. K. Jena, S.-I. Sasaki, T. Miyasaka, H. Tamiaki, X.-F. Wang, *J. Am. Chem. Soc.* **2021**, *143*, 2207.

[89] Z. Li, P. Wang, C. Ma, F. Igbari, Y. Kang, K.-L. Wang, W. Song, C. Dong, Y. Li, J. Yao, D. Meng, Z.-K. Wang, Y. Yang, *J. Am. Chem. Soc.* **2021**, *143*, 2593.

[90] L. Chu, W. Ahmad, W. Liu, J. Yang, R. Zhang, Y. Sun, J. Yang, X.'a. Li, *Nano-Micro Lett.* **2019**, *11*, 16.

[91] M. Ghasemi, M. Hao, M. Xiao, P. Chen, D. He, Y. Zhang, W. Chen, J. Fan, J. H. Yun, B. Jia, X. Wen, *Nanophotonics* **2020**, *10*, 2181.

[92] X. Yang, W. Wang, W. Ran, W. Zhou, Z. Shao, *Energy Fuels* **2020**, *34*, 10513.

[93] E. Greul, M. L. Petrus, A. Binek, P. Docampo, T. Bein, *J. Mater. Chem. A* **2017**, *5*, 19972.

[94] F. Igbari, R. Wang, Z.-K. Wang, X.-J. Ma, Q. Wang, K.-L. Wang, Y. Zhang, L.-S. Liao, Y. Yang, *Nano Lett.* **2019**, *19*, 2066.

[95] W. Gao, C. Ran, J. Xi, B. Jiao, W. Zhang, M. Wu, X. Hou, Z. Wu, *ChemPhysChem* **2018**, *19*, 1696.

[96] M. Pantaler, K. T. Cho, V. I. E. Queloz, I. García Benito, C. Fettkenhauer, I. Anusca, M. K. Nazeeruddin, D. C. Lupascu, G. Grancini, *ACS Energy Lett.* **2018**, *3*, 1781.

[97] M. Wang, P. Zeng, S. Bai, J. Gu, F. Li, Z. Yang, M. Liu, *Sol. RRL* **2018**, *2*, 1800217.

[98] G. Longo, S. Mahesh, L. R. V. Buizza, A. D. Wright, A. J. Ramadan, M. Abdi-Jalebi, P. K. Nayak, L. M. Herz, H. J. Snaith, *ACS Energy Lett.* **2020**, *5*, 2200.

[99] M. T. Sirtl, F. Ebadi, B. T. Gorkom, P. Ganswindt, R. A. J. Janssen, T. Bein, W. Tress, *Adv. Optical Mater.* **2021**, 2100202.

[100] E. Zimmermann, K. K. Wong, M. Müller, H. Hu, P. Ehrenreich, M. Kohlstädt, U. Würfel, S. Mastroianni, G. Mathiazhagan, A. Hinsch, T. P. Gujar, M. Thelakkat, T. Pfadler, L. Schmidt-Mende, *APL Mater.* **2016**, *4*, 91901.

[101] J. A. Christians, J. S. Manser, P. V. Kamat, *J. Phys. Chem. Lett.* **2015**, *6*, 852.

[102] E. Unger, G. Paramasivam, A. Abate, *J. Phys. Energy* **2020**, *2*, 44002.

[103] M. Ghasemi, L. Zhang, J. H. Yun, M. Hao, D. He, P. Chen, Y. Bai, T. Lin, M. Xiao, A. Du, M. Lyu, L. Wang, *Adv. Funct. Mater.* **2020**, *30*, 2002342.

[104] T. Luo, Y. Zhang, X. Chang, J. Fang, T. Niu, J. Lu, Y. Fan, Z. Ding, K. Zhao, S. Liu, *J. Energy Chem.* **2021**, *53*, 372.

[105] X. Yang, Y. Chen, P. Liu, H. Xiang, W. Wang, R. Ran, W. Zhou, Z. Shao, *Adv. Funct. Mater.* **2020**, *30*, 2001557.

[106] B. Wang, L. Yang, C. Dall'Agnese, A. K. Jena, S.-I. Sasaki, T. Miyasaka, H. Tamiaki, X.-F. Wang, *Sol. RRL* **2020**, *4*, 2000166.

[107] I. Chung, B. Lee, J. He, R. P. H. Chang, M. G. Kanatzidis, *Nature* **2012**, *485*, 486.

[108] M.A.K.L. Dissanayake, T. Jaseetharan, G.K.R. Senadeera, B.-E. Mellander, I. Albinsson, M. Furlani, J.M.K.W. Kumari, *J. Photochem. Photobiol., A* **2021**, *405*, 112915.

[109] A. H. Slavney, L. Leppert, D. Bartesaghi, A. Gold-Parker, M. F. Toney, T. J. Savenije, J. B. Neaton, H. I. Karunadasa, *J. Am. Chem. Soc.* **2017**, *139*, 5015.

[110] A. H. Slavney, L. Leppert, A. Saldivar Valdes, D. Bartesaghi, T. J. Savenije, J. B. Neaton, H. I. Karunadasa, *Angew. Chem., Int. Ed.* **2018**, *57*, 12765.

[111] K. P. Lindquist, S. A. Mack, A. H. Slavney, L. Leppert, A. Gold-Parker, J. F. Stebbins, A. Salleo, M. F. Toney, J. B. Neaton, H. I. Karunadasa, *Chem. Sci.* **2019**, *10*, 10620.

[112] F. Schmitz, K. Guo, J. Horn, R. Sorrentino, G. Conforto, F. Lamberti, R. Brescia, F. Drago, M. Prato, Z. He, U. Giovanella, F. Cacialli, D. Schlettwein, D. Meggiolaro, T. Gatti, *J. Phys. Chem. Lett.* **2020**, *11*, 8893.

[113] T. Appadurai, S. Chaure, M. Mala, A. K. Chandiran, *Energy Fuels 35*, 11479.

[114] Y. Li, Z. Shi, L. Lei, S. Li, D. Yang, D. Wu, T. Xu, Y. Tian, Y. Lu, Y. Wang, L. Zhang, X. Li, Y. Zhang, G. Du, C. Shan, *Adv. Mater. Interfaces* **2019**, *6*, 1900188.

Jonas Horn is a Ph.D. candidate in the group of D. Schlettwein investigating contact formation and interfacial properties of lead-free perovskite materials. During the work for his M.Sc. thesis in physics, he worked on charge carrier dynamics in perovskite solar cells using femtosecond pump probe spectroscopy.

Derck Schlettwein obtained his Ph.D. degree in physical chemistry from Bremen University and since 2004 has been a professor at the Institute of Applied Physics at Justus Liebig University Giessen. He leads a group focused on organic semiconductors and hybrid materials. They study the preparation and characterization of thin films for organic thin-film transistors and LEDs, electrochromic devices, and for dye-sensitized or perovskite solar cells.